crystals

MDPI

Article

Micro-Raman Spectroscopy Study of Vertical GaN Schottky Diode

Atse Julien Eric N'Dohi [1], Camille Sonneville [1,*], Soufiane Saidi [1], Thi Huong Ngo [2], Philippe De Mierry [2], Eric Frayssinet [2], Yvon Cordier [2], Luong Viet Phung [1], Frédéric Morancho [3], Hassan Maher [4] and Dominique Planson [1]

1 Univ. Lyon, Université Claude Bernard Lyon 1, INSA Lyon, Ecole Centrale Lyon, CNRS, Ampère, UMR5005, 69621 Villeurbanne, France
2 CNRS, CRHEA, Université Côte d'Azur, 06560 Valbonne, France
3 LAAS-CNRS, Université de Toulouse, CNRS, UPS, 31031 Toulouse, France
4 LN2-CNRS-UMI, Université de Sherbrooke, Sherbrooke, QC J1K 2R1, Canada
* Correspondence: camille.sonneville@insa-lyon.fr

Abstract: In this work, the physical and the electrical properties of vertical GaN Schottky diodes were investigated. Cathodo-luminescence (CL), micro-Raman spectroscopy, SIMS, and current-voltage (I-V) measurements were performed to better understand the effects of physical parameters, for example structural defects and doping level inhomogeneity, on the diode electrical performances. Evidence of dislocations in the diode epilayer was spotted thanks to the CL measurements. Then, using 2D mappings of the E_2^h and A_1 (LO) Raman modes, dislocations and other peculiar structural defects were observed. The I-V measurements of the diodes revealed a significant increase in the leakage current with applied reverse bias up to 200 V. The combination of physical and electrical characterization methods indicated that the electrical leakage in the reverse biased diodes seems more correlated with short range non-uniformities of the effective doping than with strain fluctuation induced by dislocations.

Keywords: cathodo-luminescence; micro-Raman spectroscopy; current-voltage I-V; GaN Schottky diodes; power electronic devices

Citation: N'Dohi, A.J.E.; Sonneville, C.; Saidi, S.; Ngo, T.H.; De Mierry, P.; Frayssinet, E.; Cordier, Y.; Phung, L.V.; Morancho, F.; Maher, H.; et al. Micro-Raman Spectroscopy Study of Vertical GaN Schottky Diode. *Crystals* **2023**, *13*, 713. https://doi.org/10.3390/cryst13050713

Academic Editors: Yangfeng Li, Zeyu Liu, Mingzeng Peng, Yang Wang, Yang Jiang, Dmitri Donetski and Yuanpeng Wu

Received: 8 March 2023
Revised: 7 April 2023
Accepted: 20 April 2023
Published: 22 April 2023

1. Introduction

Gallium nitride (GaN) has attracted much attention for their potential applications in high voltage electronic devices due to their superior physical properties, such as a wide band gap energy, high electron mobility, large breakdown field, and high thermal conductivity [1,2]. To date, commercially available lateral GaN power devices such as high-electron-mobility transistors (HEMTs) fabricated on foreign substrates have shown good and effective electrical performance [3]. However, for most of industrial GaN-on-Silicon HEMTs, this performance is still limited to a breakdown voltage of 650 V. This limitation is attributed to the reported lattice-mismatch-induced dislocations and thermo-elastic strain resulting in a limited thickness of the buffer layer. Vertical GaN devices are reported to be more suitable for high power applications versus lateral ones [4,5]. Indeed, it has been shown that a vertical structure is the most efficient way to increase both the breakdown voltage (BV) and the current density. Moreover, vertical devices should be less sensitive to surface states contrary to HEMTs. In order to achieve these performances, critical aspects such as high structural quality of the drift region, doping control, and its homogeneity need to be addressed. This is possible through an efficient use of physical and electrical characterization approaches. Recent studies have been carried out to examine the crystalline properties and electrical behavior of vertical GaN Schottky concomitantly. Ren et al. observed that the microstructure of the GaN layers and electrical properties of Schottky Barrier Diodes (SBDs) were strongly dependent on the epitaxial growth rates. By optimizing the growth conditions, they obtained a high structural quality GaN drift layer

with high mobility [4]. Tompkins et al. have also shown that deep acceptor states associated with carbon lead to a decrease in the breakdown while increasing the specific on-resistance in the GaN SBDs grown at 100 Torr [6]. Other research groups mentioned the effect of threading dislocations and the doping concentration on the electrical behavior of GaN vertical PN diodes [7,8]. Nonetheless, a clear physical understanding of the correlation between the microstructural properties and the electrical performance of the device is still not widely established.

In this work, non-destructive physical characterizations such as cathodo-luminescence (CL) and micro-Raman spectroscopy were performed and coupled with electrical characterization (reverse and forward I–V) to assess the effects of structural and electrical defects on the electrical performance of the vertical GaN SBDs. Indeed, dislocation clusters can be highlighted by CL measurements, due to their non-radiative recombination activity, and the structural defects [9] and the *n*-doping concentration distribution [10] can be probed by 2D mapping Raman spectroscopy. In this study, the E_2^h peak position and width were tracked to analyze the structural defects and stress distribution and the A_1 (LO) peak position and intensity are used to determine the *n* carrier concentration and homogeneity. Moreover, the I-V measurements were performed to check electrical performance of the SBDs. The combination of physical and electrical characterization methods indicated that the electrical leakage in the reverse biased diodes seems more correlated with short range non-uniformities of the effective doping than with the strain fluctuation induced by the dislocations.

2. Materials and Methods

A 5 µm Si *n*-doped layer was grown by MOCVD (Metal Organic Chemical Vapor Deposition) method on a GaN HVPE freestanding substrate from Saint-Gobain Lumilog [11]. GaN films were grown in a close-coupled showerhead reactor. Ammonia, trimethylgallium (TMGa), and hydrogen carrier gas were used to grow the films at 1020 °C at a growth rate of 2 µm.h^{-1}. Diluted silane was added to the vapor phase in order to dope the GaN film. The effective doping concentration value amounts to $N_d - N_a = 8 \times 10^{15}$ cm^{-3} and was determined by mercury probe capacitance-voltage (C-V) technique [12]. First, 40 nm thick rectangular Ni frames were defined by photolithography, electron beam deposition, and lift off. Then, CL measurements were performed before any contact deposition. The Schottky contact (Ni/Au) and the backside ohmic contact (Ti/Al/Ni/Au) were electron beam deposited (Figure 1a). The diodes were mesa-isolated by chlorine-based reactive ion etching. Four SBDs with different diameters (200 µm, 100 µm, and 50 µm) were fabricated on each nickel frame (Figure 1b). C-V measurements performed on these Schottky diodes confirm the previously determined concentration in the epilayer [12].

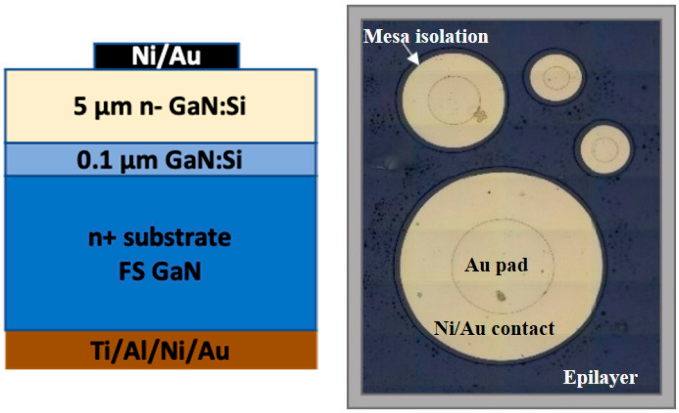

Figure 1. (**a**) Cross section of the vertical GaN Schottky diodes; (**b**) Optical microscope view of the fabricated diodes with 50 µm, 100 µm, and 200 µm diameter.

Micro-Raman spectroscopy measurements were carried out at room temperature using a confocal spectrometer (Renishaw Invia model) in back scattering geometry with a ×100 objective and a 2400 L/mm diffraction grating and a 532 nm laser excitation. The micro-Raman measurements were carried out after the complete removal of the Ni/Au Schottky contact by chemical etching. The spectral and spatial lateral resolutions were found to be around 0.1 cm^{-1} and 1 µm, respectively, and the depth resolution was between 3 and 5 µm. For the Raman measurements, 2D Raman maps were made on the epilayer of the diodes after the metallization removal. During 2D Raman measurements, cartographies of 500 × 350 µm size with a step size of 5 µm were performed on each frame containing the diodes. From these measurements, a series of E_2^h and A_1 (LO) Raman spectra were obtained and fitted using a mixed Gaussian–Lorentzian function with the Wire^{TM} Renishaw software (Figure 2). From these fitting, we extracted the values of E_2^h and A_1 (LO) peak position and intensity to create the Raman maps that were used to probe the physical properties of the diodes.

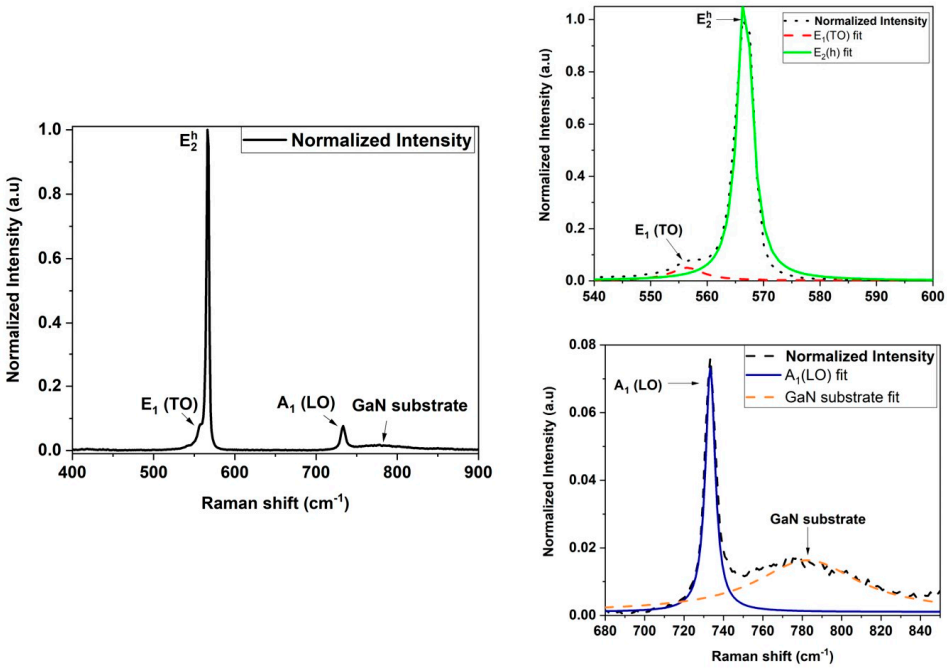

Figure 2. Raman spectrum of the diode epilayer (**left**). Right: fitted curves of E_2^h (**upper right**) and A_1 (LO) modes (**lower right**).

The CL images were recorded at room temperature using an acceleration voltage of 10 kV and a magnification of ×500 or ×1000. By inspection of 15 CL images, the dislocation density was found to be 5–10 × 10^6 cm^{-2} in 187 × 500 μm^2 areas [12]. This technique allows us to inspect the arrangement of dislocations in the GaN epilayers before the fabrication of metal contacts.

3. Results

3.1. SIMS Characterization

The SIMS measurements were conducted to examine the amount of impurities in the drift layer of the diodes and previously described in reference [13]. Figure 3 illustrates the SIMS depth profile for the Si-doped GaN film. The presence of background impurities such as carbon and oxygen can clearly be seen in the drift layer. The SIMS profile shows a very high Si concentration from the surface to about 100 nm dept. This has been previously reported in the following references [13–15] and can be explained by surface dopant atom contamination (see reference [13] for more details). After a 100 nm depth, the SIMS profile shows a uniform Si doping density (~2.5 × 10^{16} cm^{-3}) corresponding to the *n*-doped GaN epilayer grown by MOCVD. Beyond the depth of 4.2 µm, a high concentration of Si is

observed corresponding to a 100 nm thin layer of highly doped Si GaN. This high-doped layer is regrown during the MOCVD process on top of the freestanding GaN substrate to avoid interface contaminations such as carbon impurities that limit the series resistance. For this reason, high concentration of Si dopants is present in this region located beyond the depth of 4.2 µm. Finally, the 4.5 µm depth corresponds to the freestanding GaN substrate, as the substrate is doped with oxygen and the HVPE process limits the amount of carbon. Overall, the SIMS results reveal that the silicon concentration is almost uniform (~2.5 × 10^{16} cm^{-3}) in the GaN active layer. The SIMS results highlighted that the presence of carbon and oxygen impurities is not negligible. From the surface down to a 4 µm depth in the epilayer, the O and C concentrations are constant. Oxygen is a shallow donor and is present in the films due to the contamination from ammonia source [16]. On the other hand, carbon is a deep acceptor and its presence in the film is due to the decomposition of TMGa methyl groups during MOCVD process [17]. Hence, some compensation effects of the Si and O donors by the C acceptors may occur.

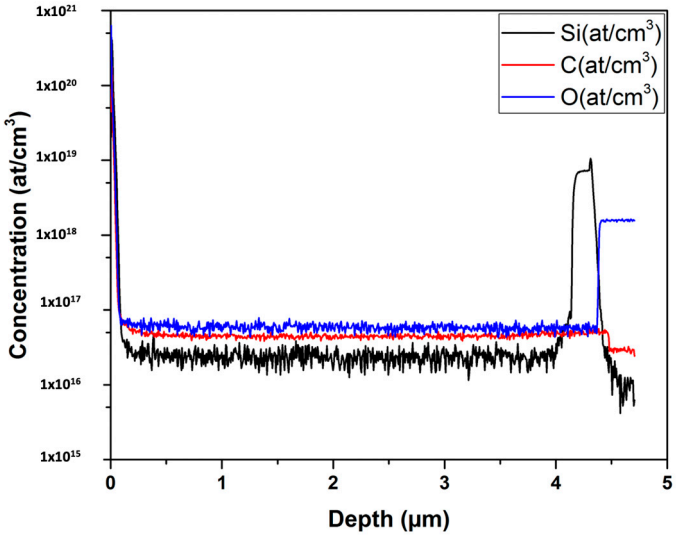

Figure 3. SIMS profiles measurement from the studied GaN vertical structure. The black curve highlights the presence of Si dopants (main dopant). The red and blue curves represent the main background impurities in the sample (carbon and oxygen respectively).

3.2. Study of the $E_2{}^h$ Peak Behavior

In epitaxial GaN, the stress is biaxial and the E_2^h mode is reported to be sensitive to the biaxial stress [18] and useful to probe crystalline quality as well; its non-polar nature makes all atoms vibrate in the x-y plane. With this mode, any effect on the atomic bonds in the lattice can be effectively sensed. Therefore, a shift of this mode indicates the level or the type of stress in the epilayer and can be accounted by Equation (1): [18]

$$\Delta\omega = K\sigma_{xx=yy} \quad (1)$$

where $\Delta\omega$ is the shift of phonon line (cm^{-1}), $\sigma_{xx=yy}$ (GPa) is the biaxial stress and K (cm^{-1}/GPa) is the pressure coefficient or the stress coefficient. That expression is useful to quantify the residual stress in the samples as long as the pressure coefficient is known. We did not evaluate the stress due to the scattered value of K in the literature [18–20]. Here, by investigating the E_2^h 2D Raman maps obtained as described earlier in the experimental method on each Ni frame, the stress and the crystal quality of the diodes drift layer were assessed. Actually, the wafer containing the homo-epi-structure was cut into two parts. The first sample contains frames 1 and 2 while the second sample contains frames 3 and 4. Figure 4 shows the E_2^h Raman maps and the CL maps (respectively in black and white) performed on the four different frames on the GaN wafer.

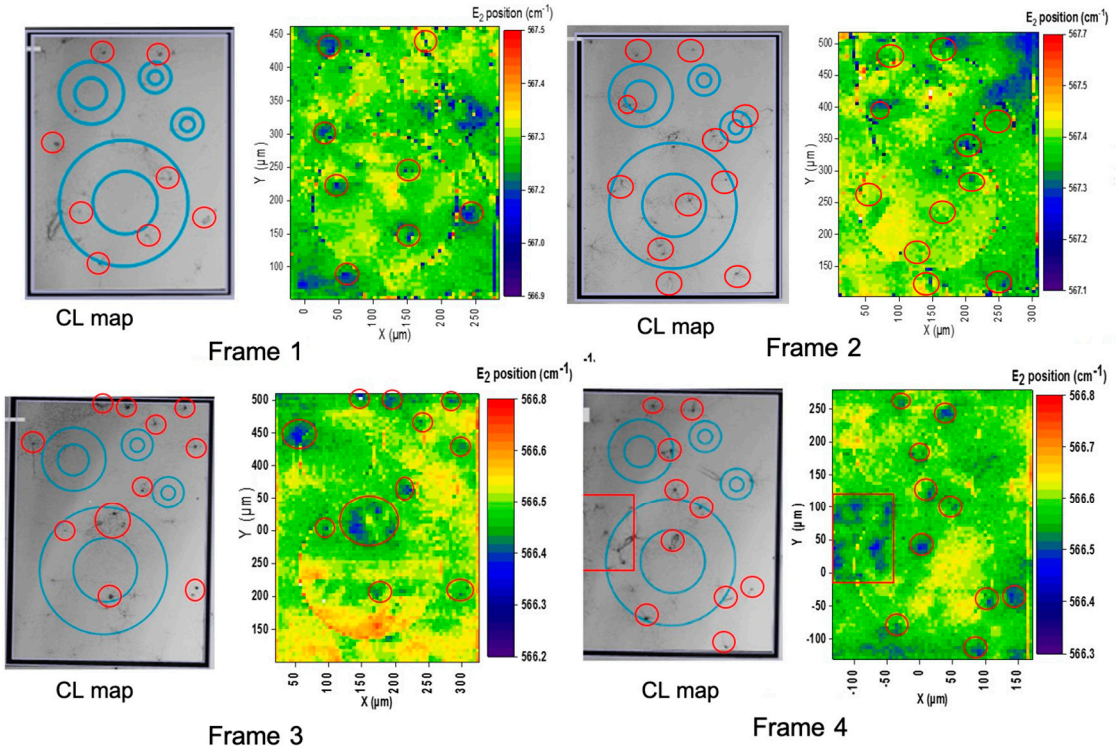

Figure 4. 2D Raman maps of E_2^h peak position (right) and their corresponding cathodo-luminescence images (in black and white, left) performed on the four frames. The red circles and rectangle are ascribed to dislocations clusters. The blue circles correspond to the areas where Schottky diodes were fabricated afterwards.

Table 1 summarizes the supporting quantification results extracted from the E_2^h position and width maps obtained by fittings. We clearly see in the Table 1 the difference in the E_2^h position mean value. Frames 1 and 2 have the E_2^h position mean value between 567.3 and 567.4 cm^1 range while frames 3 and 4 show a lower shift between 566.5 and 566.6 cm^{-1}. That difference of about 0.8 cm^{-1} may be due to the long range inhomogeneities of the original sample or to the fact that frames 3 and 4 have undergone many physical experiments such as SEM, I-V, Raman, and temperature measurements: It may have been structurally deteriorated by these operations. Therefore, we did not examine the A_1(LO) Raman map of these samples. According to Equation (1) and assuming that the mean value corresponds to the strain relaxed state, we can see on the E_2^h position maps a shift below (toward the blue zone) or above (toward the red zone) the mean value, which indicates a tensile or compressive stress, respectively. From the comparison between the E_2^h position maps and the CL image, we identified the presence of the dislocation clusters. Indeed, the observed dislocations in the CL image match well zone by zone with a shift of the E_2^h peak to a lower position in the Raman map (Figure 4). These results established a good correlation between the Raman spectroscopy and CL and therefore proves the efficiency of the micro-Raman spectroscopy as a non-destructive tool to highlight the presence of dislocations clusters as reported previously by Kokubo et al. [21]. Generally, three types of threading dislocations exist: the edge dislocations (TEDs), the screw dislocations (TSDs), and the mixed dislocations (edge and screw) (TMDs). In references [21,22] it has been reported that the TSDs do not affect the E_2^h peak shift because the shear strain has less influence on the E_2^h shift. Thus, the screw type dislocations are not detectable by means of the Raman peak shift. However, it is still challenging to distinguish the TED from the TMD types when they are both present in a GaN sample. In these previous studies, the dislocations appear as zones affected by a shift of the E_2^h peak position to a higher position close to a zone with a shift of the E_2^h peak position to a lower position. In our study, it seems that the observed dislocation clusters appear only in blue on the Raman E_2^h position map

and then correspond to an area with a lower stress. This reveals that the dislocation clusters may induce a tensile stress in the drift layer of the studied diodes. In addition, it is possible that either the step used for our mapping is too large to observe the compressive stress or that the dislocations observed here are dislocation clusters locally decreasing the stress in a similar way as the dislocations associated with the grain boundaries [23]. From the E_2^h width maps (not presented here, results summarized in Table 1), we see that the frames present peak widths with the same order of magnitude (3.6∼ 3.7 cm^{-1}). In frames 1 and 2, the value of v = 3.6 cm^{-1} can be noticed while in frames 3 and 4 the value of v = 3.7 cm^{-1} is obtained. We note a small E_2^h width gap shift of 0.1 cm^{-1} among the frames. This gap shift is insignificant to account for an effective crystalline inhomogeneity in the frames. Hence, we can tentatively infer that the crystalline structure of the drift layer is homogeneous over the whole epi wafer. Moreover, from the reference [24], the value up to v = 3.7 cm^{-1} indicates that the Si-doped epilayer is of good crystalline quality.

Table 1. E_2^h position and width quantification result.

Frame Name	E_2^h Position (Mean Value) (cm^{-1})	E_2^h Width (Mean Value) (cm^{-1})
Frame 1	567.3 ± 0.1	3.6 ± 0.1
Frame 2	567.4 ± 0.1	3.6 ± 0.1
Frame 3	566.5 ± 0.1	3.7 ± 0.1
Frame 4	566.6 ± 0.1	3.7 ± 0.1

3.3. Study of the A_1 (LO) Peak Behavior

The A_1(LO) phonon mode is used to measure the spatial distribution of the free-carrier concentration and carrier mobility of polar semiconductors such as GaN due to the interaction between the longitudinal optical (LO) phonon modes and the collective oscillation of free carriers (plasmons) that forms the LO Phonon-Plasmon coupled (LOPC) mode [25–27]. The shift in the A_1 (LO) position is known to reflect changes in the plasma frequency and enables to estimate the free-carrier density and/or mobility. The evaluation and the optimization of the carrier concentration of the GaN-based device drift layer is important for their electrical performance. By tracking the A_1 (LO) position shift through a Raman mapping, we determined the effective carrier concentration of the diodes. It has been reported that for *n*-doped GaN layers with a *n* concentration below 10^{17} cm^{-3}, the A_1 (LO) position shift is a linear function of the carrier concentration through Equation (2) [28]:

$$\omega_1 = 1.410^{-17}\, n + \omega_0 \quad (2)$$

where *n* is the *n*-carrier concentration, $\omega_1(A_1(LO))$ is the Raman shift in cm^{-1} and ω_0 is an offset value of 733.3 cm^{-1} deduced from the plot. This means that any A_1 (LO) position shift corresponds to a specific carrier concentration. As mentioned above, only frames 1 and 2 were considered in this part. From the A_1(LO) 2D position maps as displayed in Figure 5, this implies that the *n*-carrier mean concentration does not significantly vary across the region containing these frames. The doping is therefore rather homogeneous all over the region. This value corresponds to nearly $n = 7 \times 10^{15}$ cm^{-3} (Table 2) as an estimated carrier concentration using Equation (2). We clearly realize that we find a similar concentration as determined by the capacitance-voltage (C-V) mercury probe method ($n = 8 \times 10^{15}$ cm^{-3}). Therefore, we observe a good correlation between the Raman spectroscopy and the C-V method in terms of the carrier concentration evaluation.

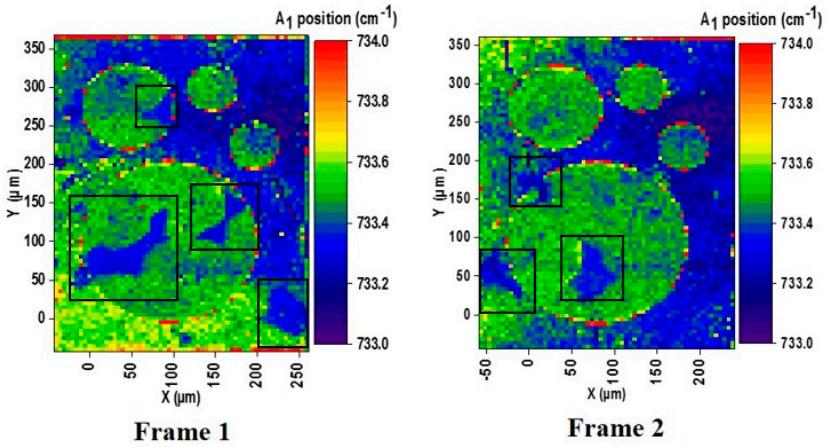

Figure 5. 2D Raman maps of A_1(LO) peak position of frames 1 and 2. The black squares are ascribed to peculiar patches.

Table 2. A_1(LO) position and *n*-carrier concentration quantification result.

Frame Name	A_1(LO) Position (Mean Value) (cm^{-1})	A_1(LO) Width (Mean Value) (cm^{-1})
Frame 1	733.4 ± 0.1	$7.1 \times 10^{15} \pm 10\%$
Frame 2	733.4 ± 0.1	$7.1 \times 10^{15} \pm 10\%$

Moreover, when considering both the A_1(LO) intensity and the position maps of frame 1 and 2 (Figures 5 and 6), we observe peculiar patches (highlighted in black squares) in the active area of the 200 µm diodes. These patches did not appear in the E_2^h maps as shown in Figure 3. Therefore, as no local strain changes are noticed, these patches cannot be ascribed to dislocations. Rather, these patches may stand for the inhomogeneous incorporation of impurities (such as carbon) during the MOCVD growth process. In these peculiar patches, the A_1(LO) intensity increases (red part) while the Raman shift position decreases (blue zone) as shown in Figures 5 and 6. As a result, they seem to affect the doping and its homogeneity in the diodes by apparently locally decreasing either the *n*-free-carrier concentration or their mobility. According to the SIMS results, they may correspond to local changes in the incorporation of silicon or background impurities such as oxygen (O) or carbon (C) or to an agglomeration of them since they all exist together in the probed epilayer thickness (5 µm). Further analyses such as EBIC [29,30] are needed to determine the exact nature of the defects that create this kind of inhomogeneity.

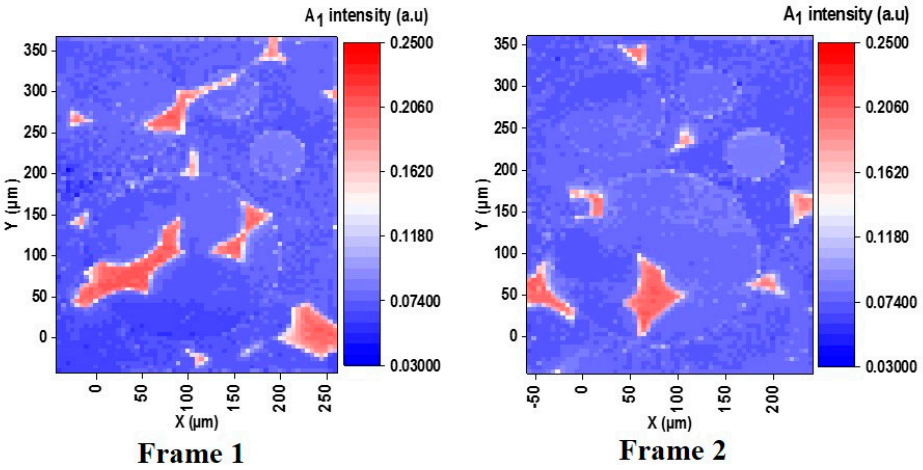

Figure 6. 2D Raman maps of A_1(LO) peak intensity of frames 1 and 2.

3.4. Electrical Characterization

The electrical behavior of the vertical SBDs was investigated through the I-V forward measurements. Figure 7 shows the result of the forward I-V characterization obtained on the four frames, containing four diodes each. The 50 µm (high) and 50 µm (low) refer to the respective location of the 50 µm diameter diodes in each Ni frame. We notice that the current density in the diodes have all the same exponential dependence when the voltage increases from 0.1 V to 0.4 V. It also shows that they are dominated by the same forward current conduction mechanism independently of the diode size. The exponential part of the I–V curves can be explained by the thermonic emission model. In this region, the current density J can be expressed with the following equation [31]:

$$J = \mathrm{A^*T^2} \exp\left(-\frac{q\phi_B}{\mathrm{kT}}\right) \exp\left(\frac{q\mathrm{V}}{n\mathrm{kT}}\right) \quad (3)$$

where A* is the GaN Richardson's constant for GaN, T is the temperature, ϕ_B is the Schottky barrier height (SBH), k is the Boltzmann constant, V is the applied bias voltage, q is the elementary charge, n is the ideality factor. When the forward bias is beyond 0.4 V, the increase in the current density is limited by the series resistance, and Equation (3) should be modified. From Equation (3), applied to the linear region of the log(J)-V curve, we deduce the ideality factor from the intercept and the barrier height from the slope. Table 3 summarizes the values obtained for n and Φ_B. All the diodes show the typical Schottky behavior with the ideality factor close to the unity and varying from 1.01 up to 1.19, independently of the diode size. The barrier heights are between 0.74 V and 0.91 V and seem to increase with the diode size.

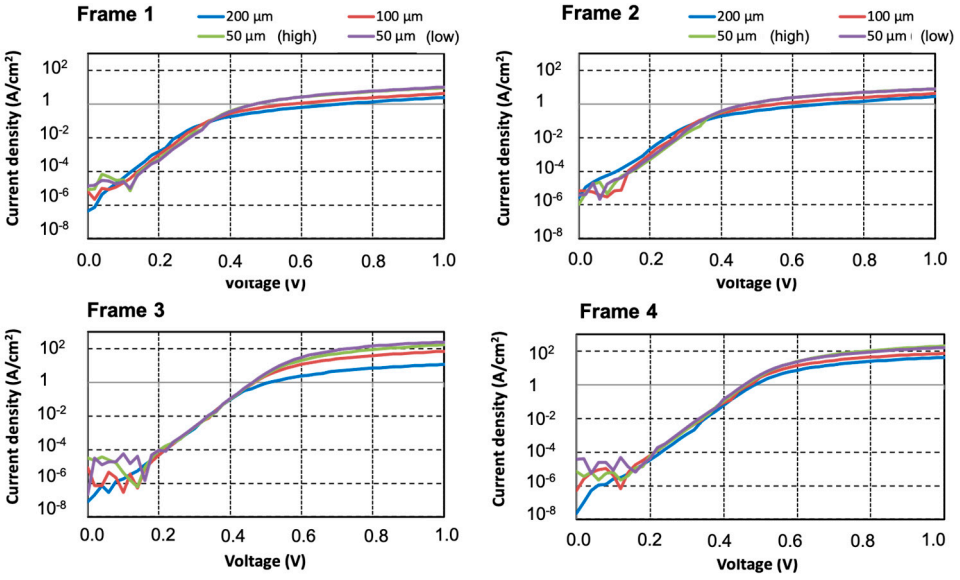

Figure 7. Forward I-V characteristics for diodes from the frames (1, 2, 3 and 4): blue (200-µm diode), red (100-µm diode), green (50-µm high), purple (50-µm low).

The diode electrical behavior was investigated through the I–V reverse measurements down to −200 V. Figure 8 shows the result of the reverse I–V characterization. All the studied diodes on the wafer display nearly the same reverse characteristics with a relatively high leakage current density ranging between 10^{-3} and 10^{-1} A.cm^{-2} at −200 V. The third column of Table 3 summarizes the reverse voltage (V_r), at which a leakage current density of 0.5 10^{-2} A.cm^{-2} is reached. This voltage varies between −70 V and −185 V. The lower V_r is obtained for the diodes of frames 1 and 2 and the higher V_r for the diodes of frames 3 and 4. However, V_r seems to be independent of the diode size. Then we suspect that the observed dispersion between frames may be caused by the presence of some structural defects (such

as dislocations) or electrical defects in the drift layer. These defects may actively play a major role in the performance of the diodes by somehow influencing the net carrier distribution across the drift layer.

Table 3. Ideality factor (n) and Schottky barrier height (ϕ_B) deduced from the I-V forward measurements and V_r (reverse voltage at current density J = 0.5 mA/cm^2).

Frame Name, Diode Size (µm)	n	ϕ_B (*Volt*)	V_r (V)
Frame 1, 200	1.08	0.74	−110 V
Frame 1, 100	1.03	0.80	−125 V
Frame 1, 50 (high)	1.07	0.83	−120 V
Frame 1, 50 µm (low)	1.11	0.83	−150 V
Frame 2, 200	1.17	0.72	−70 V
Frame 2, 100	1.09	0.78	−125 V
Frame 2, 50 (high)	1.13	0.82	NONE
Frame 2, 50 (low)	1.09	0.82	−155 V
Frame 3, 200	1.03	0.83	−180 V
Frame 3, 100	1.01	0.87	−170 V
Frame 3, 50 (high)	1.08	0.88	−175 V
Frame 3, 50 µm (low)	1.07	0.89	−180 V
Frame 4, 200	1.03	0.84	−185 V
Frame 4, 100	1.09	0.85	−160 V
Frame 4, 50 µm (high)	1.00	0.91	−180 V
Frame 4, 50 µm (low)	1.00	0.91	−175 V

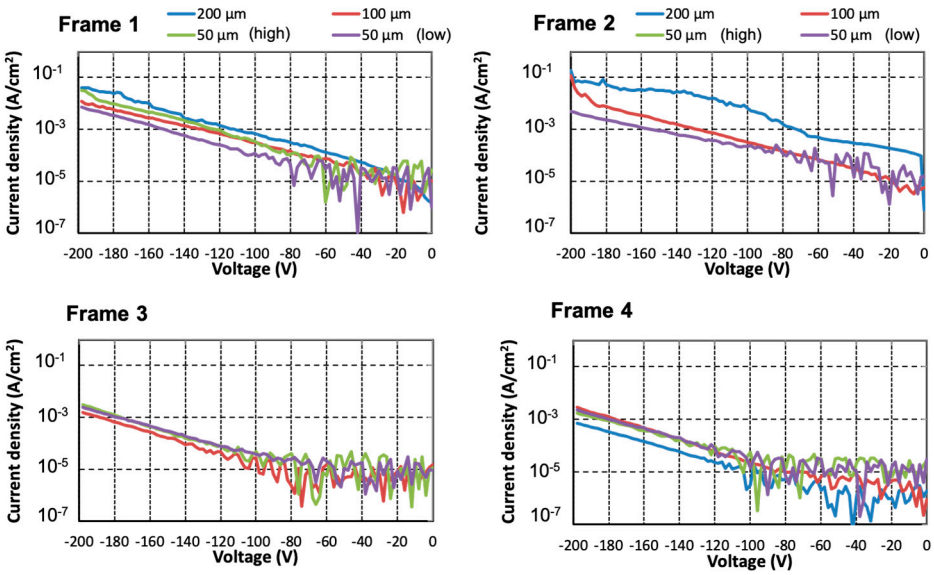

Figure 8. Reverse I-V characteristics for diodes from the frames (1, 2, 3 and 4): blue (200 µm diode), red (100 µm diode), green (50 µm high), purple (50 µm diode low).

4. Discussion

The E_2^h Raman position maps correlate well with the cathodo-luminescence measurements (see Figure 4), showing that the Raman spectroscopy can be used to localize the threading dislocations in the GaN active layer. Our measurements reveal that the dislocation clusters may locally decrease the stress in a similar way as the dislocations associated with the grain boundaries. In addition, the 2D A_1(LO) position and intensities maps were used to estimate the carrier concentration in the diodes and identify peculiar defects. Figures 5 and 6

show that the area occupied by the defects is particularly important with respect to the diode size for the two 200 µm diodes of frames 1 and 2. These peculiar defects locally decrease the net carrier concentration and therefore may possibly affect the Schottky diode electrical performances. The SIMS results highlighted the presence of a significant amount of oxygen and carbon, and the changes in the incorporation of silicon or of these impurities could explain the observed variation of the ***n***-carrier concentration. The I-V forward characterizations show that all the studied diodes have a typical Schottky behavior with ideality factors between 1 and 1.17. The I-V reverse characterizations show that all the studied diodes have leakage currents increasing with the applied reverse voltage and they are higher for the diodes of frame 1 and 2, especially for the two 200 µm diodes. These results seem to indicate that the defects observed in the A_1(LO) Raman maps (Figures 5 and 6) are electrically active and contribute to the reverse leakage. Thus, the electrical leakage in the reverse biased diodes seems more correlated with the short range non-uniformities of the effective doping rather than with the strain fluctuation induced by the dislocations, a result in agreement with our previous investigations on dislocation clusters [12].

5. Conclusions

In this work, vertical GaN Schottky diodes on a freestanding GaN substrate were fabricated and investigated. The physical and the electrical properties were studied with cathodo-luminescence, micro-Raman mapping, SIMS measurements, and current-voltage (I-V) to understand the effects of physical parameters such as threading dislocations and doping concentration homogeneity on the electrical performances of SBDs. Evidence of dislocations in the diode epilayer was spotted thanks to CL measurements and a correlation with 2D mappings of the Raman $E_2{}^h$ signal was observed. The I-V measurements of the diodes reveal a significant increase in the leakage current with applied reverse bias up to 200 V. However, no clear correlation with the presence of dislocation cluster in the area occupied by the diodes and excessive leakage current were observed. On the contrary, the mapping of the A1 (LO) Raman mode that is sensitive to fluctuations of the effective doping level shows correlations with the leakage. Even when the origin of such fluctuations remains to be identified, this study shows the efficiency of micro-Raman spectroscopy to probe structural and electronic properties of GaN-based electrical vertical devices. The combination of physical and electrical characterization methods indicates that the electrical leakage in the reverse biased diodes seems more correlated with short range non-uniformities of the effective doping than with the strain fluctuation induced by the dislocations and thus, this method can be efficient to study vertical GaN electrical power devices. Finally, we suggest further investigations such as DLTS measurements to set up a solid correlation between physical properties and the observed electrical behavior of the diodes [13].

Author Contributions: Data curation, A.J.E.N., C.S. and S.S.; formal analysis, A.J.E.N., S.S. and T.H.N.; investigation, A.J.E.N., S.S., T.H.N., P.D.M., E.F. and Y.C.; methodology, C.S., Y.C. and D.P.; project administration, L.V.P., F.M., Yvon Cordier and H.M.; supervision, C.S., H.M. and D.P.; validation, C.S. and D.P.; writing—original draft, A.J.E.N.; writing—review and editing, A.J.E.N., C.S., Y.C., L.V.P., F.M., H.M. and D.P. All authors have read and agreed to the published version of the manuscript.

Funding: This work was supported by the French Technology Facility Network RENATECH, the French National Research Agency (ANR) through the projects C-Pi-GaN (Grant No. ANR-18- CE05-0045), GaNeX (ANR-11-LABX-0014) and the AuRA Region (Région Auvergne-Rhône Alpes) through the OptiGaN project.

Data Availability Statement: The data presented in this study are available on request from the corresponding author.

Conflicts of Interest: The authors declare no conflict of interest.

References

1. Cao, Y.; Chu, R.; Li, R.; Chen, M.; Chang, R.; Hughes, B. High-voltage vertical GaN Schottky diode enabled by low-carbon metal-organic chemical vapor deposition growth. *Appl. Phys. Lett.* **2016**, *108*, 62103. [CrossRef]
2. Yeluri, R.; Lu, J.; Hurni, C.A.; Browne, D.A.; Chowdhury, S.; Keller, S.; Speck, J.S.; Mishra, U.K. Design, fabrication, and performance analysis of GaN vertical electron transistors with a buried p/n junction. *Appl. Phys. Lett.* **2015**, *106*, 183502. [CrossRef]
3. Amano, H.; Baines, Y.; Beam, E.; Borga, E.; Bouchet, T.; Chalker, P.R.; Charles, M.; Chen, K.J.; Chowdury, N.; Chu, R.; et al. The 2018 GaN power electronics roadmap. *J. Phys. D Appl. Phys.* **2018**, *51*, 163001. [CrossRef]
4. Ren, B.; Liao, M.; Sumiya, M.; Wang, L.; Koide, Y.; Sang, L. Nearly ideal vertical GaN Schottky barrier diodes with ultralow turn-on voltage and on-resistance. *Appl. Phys. Express* **2017**, *10*, 51001. [CrossRef]
5. Sang, L.; Ren, B.; Sumiya, M.; Liao, M.; Koide, Y.; Tanaka, A.; Cho, Y.; Harada, Y.; Nabatame, T.; Sekiguchi, T.; et al. Initial leakage current paths in the vertical-type GaN-on-GaN Schottky barrier diodes. *Appl. Phys. Lett.* **2017**, *111*, 122102. [CrossRef]
6. Tompkins, R.P.; Walsh, T.A.; Derenge, M.A.; Kirchner, K.W.; Zhou, S.; Nguyen, C.B.; Jones, K.A. The effect of carbon impurities on lightly doped MOCVD GaN Schottky diodes. *J. Mater. Res.* **2011**, *26*, 2895–2900. [CrossRef]
7. Fujikura, H.; Hayashi, K.; Horikiri, F.; Narita, Y.; Konno, T.; Yoshida, T.; Ohta, H.; Mishima, T. Elimination of macrostep-induced current flow nonuniformity in vertical GaN PN diode using carbon-free drift layer grown by hydride vapor phase epitaxy. *Appl. Phys. Lett. Express* **2018**, *11*, 45502. [CrossRef]
8. Usami, S.; Ando, Y.; Tanaka, A.; Nagamatsu, K.; Deki, M.; Kushimoto, M.; Nitta, S.; Honda, Y.; Amano, H.; Sugawara, Y.; et al. Correlation between dislocations and leakage current of p-n diodes on a free-standing GaN substrate. *Appl. Phys. Lett.* **2018**, *112*, 182106. [CrossRef]
9. Amilusik, M.; Wlodarczyk, D.; Suchocki, A.; Bockowski, M. Micro-Raman studies of strain in bulk GaN crystals grown by hydride vapor phase epitaxy on ammonothermal GaN seeds. *Jpn. J. Appl. Phys.* **2019**, *58*, SCCB32. [CrossRef]
10. Kozawa, T.; Kachi, T.; Kano, H.; Taga, Y.; Hashimoto, M.; Koide, N.; Manabe, K. Raman scattering from LO phonon-plasmon coupled modes in gallium nitride. *J. Appl. Phys.* **1994**, *75*, 1098. [CrossRef]
11. Gogova, D.; Larsson, H.; Kasic, A.; Yazdi, G.R.; Ivanov, I.; Yakimova, R.; Monemar, B.; Aujol, E.; Frayssinet, E.; Faurie, J.-P.; et al. High-Quality 2″ Bulk-Like Free-Standing GaN Grown by HydrideVapour Phase Epitaxy on a Si-doped Metal Organic Vapour Phase Epitaxial GaN Template with an Ultra Low Dislocation Density. *Jpn. J. Appl. Phys.* **2005**, *44*, 3R. [CrossRef]
12. Ngo, T.H.; Comyn, R.; Frayssinet, E.; Chauveau, H.; Chenot, S.; Damilano, B.; Tendille, F.; Cordier, Y. Cathodoluminescence and electrical study of vertical GaN-on-GaN Schottky diodes with dislocation clusters. *J. Cryst. Growth* **2020**, *552*, 125911.
13. Vigneshwara Rajaa, P.; Raynaud, C.; Sonneville, C.; N'Dohi, A.E.; Morel, H.; Phung, L.V.; Ngo, T.H.; De Mierry, P.; Frayssinet, E.; Maher, H.; et al. Comprehensive characterization of vertical GaN-on-GaN Schottky barrier diode. *Microelectron. J.* **2022**, *128*, 105575. [CrossRef]
14. Reshchikov, M.A.; Vorobiov, M.; Andrieiev, O.; Ding, K.; Izyumskaya, N.; Avrutin, V.; Usikov, A.; Helava, H.; Makarov, Y. Determination of the concentration of impurities in GaN from photoluminescence and secondary-ion mass spectrometry. *Sci. Rep.* **2020**, *10*, 2223. [CrossRef]
15. Freitas, J.A., Jr.; Moore, W.J.; Shanabrook, B.V.; Braga, G.C.; Lee, S.K.; Park, S.S.; Han, J.Y.; Koleske, D.D. Donors in hydride-vapor-phase epitaxial GaN. *J. Cryst. Growth* **2002**, *246*, 307–314. [CrossRef]
16. Popovici, G.; Kim, W.; Botchkarev, A.; Tang, H.; Morkoc, H. Impurity contamination of GaN epitaxial films from the sapphire, SiC and ZnO substrates. *Appl. Phys. Lett.* **1997**, *71*, 3385–3387. [CrossRef]
17. Ciarkowski, T.; Allen, N.; Carlson, E.; McCarthy, R.; Youtsey, C.; Wang, J.; Fay, P.; Xie, J.; Guido, L. Connection between Carbon Incorporation and Growth Rate for GaN Epitaxial Layers Prepared by OMVPE. *Materials* **2019**, *12*, 2455. [CrossRef]
18. Wagner, J.-M.; Bechstedt, F. Phonon deformation potentials of α-GaN and -AlN: An ab initio calculation. *Appl. Phys. Lett.* **2000**, *77*, 346–348. [CrossRef]
19. Demangeot, F.; Frandon, J.; Baules, P.; Natali, F.; Semond, F.; Massies, J. Phonon deformation potentials in hexagonal GaN. *Phys. Rev. B* **2004**, *69*, 155215. [CrossRef]
20. Wagner, J.-M.; Bechstedt, F. Properties of strained wurtzite GaN and AlN: Ab initio studies. *Phys. Rev. B* **2002**, *66*, 115202. [CrossRef]
21. Kokubo, N.; Tsunooka, Y.; Fujie, F.; Ohara, J.; Onda, S.; Yamada, H.; Shimizu, M.; Harada, S.; Tagawa, M.; Ujihara, T. Non-destructive visualization of threading dislocations in GaN by micro raman mapping. *Jpn. J. Appl. Phys.* **2019**, *58*, SCCB06. [CrossRef]
22. Belabbas, I.; Béré, A.; Chen, J.; Ruterana, P.; Nouet, G. Investigation of the atomic core structure of the (a and c)-mixed dislocation in wurtzite GaN. *Phys. Stat. Solid C* **2007**, *4*, 2940–2944. [CrossRef]
23. Dadgar, A.; Poschenrieder, M.; Reiher, A.; Bläsing, J.; Christen, J.; Krtschil, A.; Finger, T.; Hempel, T.; Diez, A.; Krost, A. Reduction of stress at the initial stages of GaN growth on Si(111). *Appl. Phys. Lett.* **2003**, *82*, 28. [CrossRef]
24. Nenstiel, C.; Bügler, M.; Callsen, G.; Nippert, F.; Kure, T.; Fritze, S.; Dadgar, A. Germanium–The superior dopant in n-type GaN. *Phys. Stat. Solidi (RRL)–Rapid Res. Lett.* **2015**, *9*, 716–721. [CrossRef]
25. Artús, L.; Cusco, R.; Ibanez, J.; Blanco, N.; Gonzalez-Dıaz, G. Raman scattering by LO phonon-plasmon coupled modes in n-type InP. *Phys. Rev. B* **1999**, *60*, 5456–5463. [CrossRef]
26. Kuball, M. Raman spectroscopy of GaN, AlGaN and AlN for process and growth monitoring/control. *Surf. Interface Anal.* **2001**, *31*, 987–999. [CrossRef]

27. Peng, Y.; Xu, X.; Hu, X.; Jiang, K.; Song, S.; Gao, Y.; Xu, H. Raman spectroscopic study of the electrical properties of 6H–SiC crystals grown by hydrogen-assisted physical vapor transport method. *J. Appl. Phys.* **2010**, *107*, 93519. [CrossRef]
28. N'Dohi, A.E.; Sonneville, C.; Phung, L.V.; Ngo, T.H.; De Mierry, P.; Frayssinet, E.; Maher, H.; Tasselli, J.; Isoird, K.; Morancho, F.; et al. Micro-Raman characterization of homo-epitaxial n doped GaN layers for vertical device applications. *AIP Adv.* **2022**, *12*, 25126. [CrossRef]
29. Bandić, Z.Z.; Bridger, P.M.; Piquette, E.C.; McGill, T.C. The values of minority carrier diffusion lengths and lifetimes in GaN and their implications for bipolar devices. *Solid-State Electron.* **2000**, *44*, 221–228. [CrossRef]
30. Pugatschow, A.; Heiderhoff, R.; Balk, L.J. Time resolved determination of electrical field distributions within dynamically biased power devices by spectral EBIC investigations. *Microelectron. Reliab.* **2007**, *47*, 1529–1533. [CrossRef]
31. Sawada, M.; Sawada, T.; Yamagata, Y.; Imai, K.; Kimura, H.; Yoshino, M.; Iizuka, K.; Tomozawa, H. Electrical characterization of n-GaN Schottky and PCVD-SiO2/n-GaN interfaces. *J. Cryst. Growth* **1998**, *189–190*, 706–710. [CrossRef]